PHYSICAL REVIEW D **81,** 103006 (2010)

Origin of the cosmic network in ΛCDM: Nature vs nurture

Sergei Shandarin,[1] Salman Habib,[2] and Katrin Heitmann[3]

[1]*Department of Physics and Astronomy, University of Kansas, Lawrence, Kansas 66045, USA*
[2]*T-2, Theoretical Division, Los Alamos National Laboratory, Los Alamos, New Mexico 87545, USA*
[3]*ISR-1, ISR Division, Los Alamos National Laboratory, Los Alamos, New Mexico 87545, USA*

(Received 23 December 2009; published 24 May 2010)

The large-scale structure of the Universe, as traced by the distribution of galaxies, is now being revealed by large-volume cosmological surveys. The structure is characterized by galaxies distributed along filaments, the filaments connecting in turn to form a percolating network. Our objective here is to quantitatively specify the underlying mechanisms that drive the formation of the cosmic network: By combining percolation-based analyses with N-body simulations of gravitational structure formation, we elucidate how the network has its origin in the properties of the initial density field (*nature*) and how its contrast is then amplified by the nonlinear mapping induced by the gravitational instability (*nurture*).

DOI: 10.1103/PhysRevD.81.103006 PACS numbers: 98.65.−r, 98.65.Dx, 98.80.−k, 98.80.Bp

I. INTRODUCTION

Observations of the large-scale distribution of galaxies have been underway for several decades [1]. Going well beyond early ''slice'' views, recent observations reveal a nontrivial three-dimensional structure [2,3]. Two key features of the structure are immediately apparent: (i) a considerable departure from local isotropy towards filamentlike concentrations of galaxies and (ii) a tendency of the filaments to connect into a single percolating network spanning the entire region of observation. (A nice visualization of the large-scale structure as observed by the Sloan Digital Sky Survey can be found in Ref. [4].) A very similar picture also emerges from cosmological N-body simulations of the gravitational instability, the root cause of structure formation in the cosmological standard model (Fig. 1).

Many statistics have been suggested and used to characterize cosmological structures. The galaxy two-point correlation function and its Fourier analog, the power spectrum, have been used extensively since the late 1960s [5,6]. As a way of studying the amplitude of density fluctuations, these two-point statistics are observationally robust and relatively straightforward to measure (in principle), as well as to predict theoretically (see, e.g., Ref. [7], and citations therein). However, being insensitive to phases, they do not contain shape information and cannot be used to probe the overall geometry and topology of the large-scale structure. The full hierarchy of n-point correlation functions, or the corresponding n-spectra, does carry complete information about the spatial distribution of galaxies. But n-point functions are difficult to measure as well as to predict. Furthermore, the desired information can be spread in a highly nontrivial manner over the space of n-point correlation functions. For these reasons, the use of higher-point statistics has been mainly restricted to the perturbative regime ($\langle(\delta\rho_R/\bar{\rho})^2\rangle^{1/2} \lesssim 1$) corresponding to smoothed fields with a relatively large smoothing scale, $R \gtrsim 5h^{-1}$ Mpc [$\bar{\rho}$ is the mean density and $\delta\rho_R$ is the density fluctuation smoothed on a scale R as defined in Eq. (2) below]. Because of the lack of a single obvious way to proceed (and depending on the particular application in mind) many different statistics have been suggested for analyzing large-scale structure observations and simulations. These include counts in cells, two- and higher order correlation functions [6], the Euler characteristic or equivalently the genus curve [8], global and partial Minkowski functionals [9], the void probability function [10], minimal spanning tree [11], and many others.

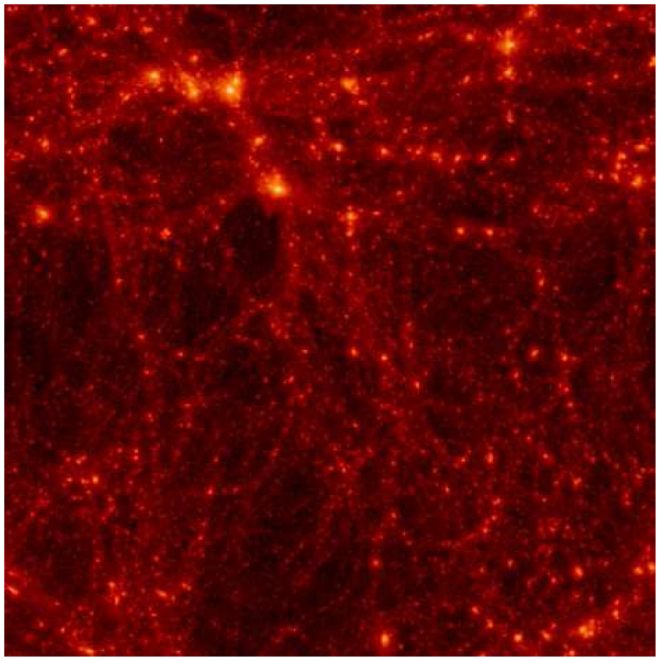

FIG. 1 (color online). Demonstration of filamentary structure in N-body simulations. The projected density field is shown for a ΛCDM cosmology, with a box size of $64h^{-1}$ Mpc.

In this work, we use percolation statistics to directly address the issue of connectedness of superclusters of galaxies resulting in the emergence of the cosmic web. Our approach is attractive for two reasons: (i) The fact that simple scaling relations can be used to describe the percolation properties of cosmic density fields and (ii) that—as we show below—particle methods can also be conveniently folded into the analysis.

The existence of the cosmic web in cosmological N-body simulations is certainly manifest (Fig. 1). In search of a more analytic understanding of the dynamical origin of the network topology, most theoretical approaches start by invoking an idea due to Zel'dovich [12,13]: approximate the full evolution by a mapping from initial Lagrangian ($\mathbf{q}$) coordinates to the final Eulerian ($\mathbf{x}$) state, via

$$\mathbf{x}(\mathbf{q}, t) = \mathbf{q} + D(t)\mathbf{s}_R(\mathbf{q}). \tag{1}$$

Here $\mathbf{x}$ are the comoving coordinates, related to physical coordinates $\mathbf{r}$ as $\mathbf{x} = \mathbf{r}/a(t)$, where $a(t)$ is the scale factor describing the uniform expansion of the universe. The vector field $\mathbf{s}_R(\mathbf{q})$ is determined by the density fluctuations smoothed on a scale R at the initial time t_i,

$$\delta_R(\mathbf{q}, t_i) \equiv (\rho_R - \bar{\rho})/\bar{\rho} = -D(t_i)\nabla\mathbf{s}_R \tag{2}$$

and the monotonically growing function $D(t)$ describes the growth of density fluctuations in the linear regime. Additional information present in the initial conditions may also be exploited, e.g., by employing the deformation tensor $d_{ik} = -\partial s_i/\partial q_k$ and higher-order tensorial derivatives [14].

The dynamical mapping (1) is single-valued during the early (linear) phase of the evolution, becoming multivalued after orbit-crossing (nonlinear phase). The initial cosmic density field is a realization of a Gaussian random process, specified completely by the associated power spectrum, $P(k)$. The choice of cosmological model fixes $a(t)$, $D(t)$, and $P(k)$. We choose to set the smoothing of the initial perturbations to the present scale of nonlinearity, $R \approx R_{\rm nl}$, such that the linear *rms* density fluctuation $\sigma(R_{\rm nl}) \equiv \langle\delta^2_{R_{\rm nl}}\rangle^{1/2} = 1$ at the present epoch. This choice of the smoothing scale is based on the observation (made in N-body simulations) that the large-scale density field is mainly determined by the linear power spectrum on the scales that have just become nonlinear, i.e., with $k \lesssim R_{\rm nl}^{-1}$ [15]. It has also been shown that eliminating the perturbations on scales $k \gtrsim R_{\rm nl}^{-1}$ by truncation of the initial spectrum [16] or by smoothing with a Gaussian filter [17] removes structures at small scales but does not have much of an effect at large scales.

One line of attack is to consider the evolution in a given realization of the initial conditions as a deterministic map, and derive the properties of the network by studying generic singularities formed during nonlinear evolution [13,14] using the deformation tensor, as well as higher order tensorial derivatives. Alternatively, one can employ a probabilistic approach, investigating network properties as determined by conditional multipoint correlation functions between certain parameters (e.g., the shear tensor) related to the deformation tensor at linear density peaks [18]. These approaches have led to valuable insights, yet neither address the global properties of the cosmic network directly. Both focus primarily on the structural building blocks (halos, filaments, pancakes) and may be loosely characterized as "local," even though the characteristic scales of interest may reach tens of Mpc.

In this paper, we take up the idea of identifying the cosmic network with percolating regions in the density field at the present time [19,20], and apply percolation statistics as a quantitative global measure of the network structure [21] at both early and late times. In cosmological applications of percolation, one studies the properties of overdense and underdense excursion sets (ES), i.e., regions where the density is greater than some value ($\rho > \rho_c$) or less ($\rho < \rho_c$). Of particular interest are the connectivity properties of the excursion sets as the threshold ρ_c is varied.

Previous studies of percolation regions in the initial Gaussian and nonlinear fields—for two spatial dimensions—assumed the dynamics described by the Zel'dovich approximation and showed that the percolation region identified at the initial stage in the linear field became a part of the percolation region identified at the nonlinear stage [22]. The major reason for this conclusion was the continuity of the mapping described by the Zel'dovich approximation. Here, we investigate the relationship between percolating regions in the initial (linear, Gaussian) and late-time evolved (nonlinear, non-Gaussian) density fields using N-body simulations of a ΛCDM cosmology. Our results establish the close—although not perfect—connection between the percolating regions in the linear and nonlinear stages of the evolution, as well as provide an understanding of the network structure based on percolation concepts.

Studies of the percolation properties of density fields obtained in cosmological N-body simulations with scale-free initial power spectra ($P(k) \propto k^n$) both in linear and nonlinear regimes have been conducted previously [23,24]. In Ref. [23] a suite of N-body simulations in the Einstein-de Sitter universe (with $n = -2, -1, 0, 1$) was used to measure the percolation transition in the mass density field at four stages of dynamical evolution. It was shown that percolation transitions in overdense and underdense excursion sets experience shifts in opposite directions from that of the initial Gaussian state (where they are obviously identical due to the symmetry of Gaussian fields with respect to the sign of the field). In general, the percolation transition in the overdense phase occurs at lower than the Gaussian values while in the underdense phase it takes place at higher values of the volume fraction (by volume fraction we mean the fraction of the total volume in the

corresponding phase). The dynamical evolution of the density field results in shrinking the percolating region in the overdense phase. At the same time the percolating region in the underdense phase gains considerably in volume. It is important to keep in mind that these are two independent statements since the overdense and underdense percolating regions have different boundaries in three-dimensional space. A statistically significant trend was found relating the spectral index n to percolation: the greater the spectral index, the greater the delay in percolation as measured by larger values of $f_{\rm p} = (V_{\rm ES}/V_{\rm tot})_{\rm at\ percolation}$, or a correspondingly lower density threshold for percolation, $\delta_{\rm p}/\sigma$. These results were in qualitative agreement with Ref. [24] which used a set of larger N-body simulations ($n = -2, -1, 0$). In the latter work, the authors investigated the topology of the overdense and underdense excursion sets at the corresponding percolation thresholds in the density fields smoothed at various scales. They also measured percolation thresholds in the initial Gaussian fields and found the thresholds to be different for density fields with different power spectra.

Our work differs from previous studies in several respects. First, we focus on the observationally realistic case of the ΛCDM model where the linear power spectrum cannot be described by a single power law (previous studies of percolation in specific cosmological models do exist, e.g., Ref. [25], however those models have since been ruled out observationally). Second, our simulation volume (both in terms of size and number of realizations) is significantly larger than considered previously. This helps to control finite size effects and reduces the statistical errors significantly. Finally, and most importantly, we consider a completely new *dynamical* problem—how does the (initial) linear percolating cluster map to the (final) nonlinear percolating cluster? By quantifying the accuracy of the mapping, we are able to distinguish between two key aspects that underlie the structure of the cosmic web—an already-present conspicuousness of the percolating region in the initial Gaussian field, which we refer to as *nature*, and the enhancement due to the gravitational instability, which we term *nurture*.

In this paper, we examine the correspondence between percolating regions in the matter density fields at the linear and nonlinear stage. Three-dimensional structure in the Universe is observed, however, via the distribution of galaxies in redshift catalogs obtained from cosmological surveys such as 2dF or SDSS. According to the modern theory of galaxy formation, galaxies are embedded in dark matter halos, with the galaxy properties and number being related to the mass and evolution history of the host dark matter halos. The host halos are known to be good, albeit biased, tracers of the underlying mass field. On the larger length scales considered here (with respect to the typical galaxy separation), percolation regions in both galaxy and dark matter distributions should be very similar.

To compute the predicted percolation properties of the galaxy distributions themselves in the ΛCDM model or for galaxy redshift surveys requires mock catalogs generated from either a statistical approach such as that of the halo occupancy distribution (HOD) or using semianalytic models of galaxy formation [26]. Aside from fundamental issues, such as how to best map the galaxy distribution into a smooth field, or to use a point-process technique (e.g., a friend-of-friends cluster finder) as a proxy for a threshold-based percolation analysis, observational issues also enter. These include such problems as dealing with observational issues such as magnitude limited catalogs, nonuniform sky coverage, etc. It is not our purpose here to present a complete scheme for how to do a percolation analysis from a galaxy catalog. Nevertheless, we note that several observational studies have been carried out that have succeeded in measuring a significant signal of filamentarity in redshift catalogs [27].

An additional theoretical complication is related to the fact that real galaxy distributions are available only in redshift space. Although mapping the structure from real to redshift space is numerically simple it requires an additional elaboration of the technique. Redshift space is fundamentally anisotropic in the sense that the statistical properties of the large-scale structure are different along the line of sight and in the orthogonal directions [28]. This will require additional refining of the technique discussed here; we therefore reserve the analysis of galaxy catalogs in redshift space for future work.

The rest of the paper is organized as follows: we first describe the cosmological models used in the study and then present results from percolation analysis of linear (Gaussian) density fields. After this we discuss the results of the percolation analysis of the evolved nonlinear (non-Guassian) density fields (filtered with the same window as the linear density fields). In the last step, we study the accuracy of the mapping of the linear percolating cluster into the nonlinear percolating cluster, and end with a summary of the main results.

II. PERCOLATION TRANSITION

A. Cosmological model

The ΛCDM cosmological model adopted here is specified by the following parameters: the dimensionless Hubble constant, $h = H_0/(100\ {\rm km/s/Mpc}) = 0.7$, dimensionless dark matter and baryon densities $\Omega_{\rm dm} = 0.259$ and $\Omega_b = 0.02h^{-2}$, primordial spectral index $n = 1$, and a $P(k)$ normalization set by $\sigma_8 = \sigma(R_{\rm TH} = 8h^{-1}\ {\rm Mpc}) = 0.84$, where $R_{\rm TH}$ is the radius of the top-hat filter—the conventional measure of the amplitude of the initial density fluctuations in cosmology. Our purpose is not to consider a model that is precisely the one given by current observations (which in any case would be a moving target), but is nonetheless close enough to have the same generic properties.

Within this cosmology, we used two ensembles differing in box size and filtering scale: 15 realizations generated in a $341.3h^{-1}$ Mpc box in linear dimension, filtered at $R = 1h^{-1}$ Mpc ($\Lambda\mathrm{CDM}_1$) and 10 realizations in a $3413h^{-1}$ Mpc box, filtered at $R = 10h^{-1}$ Mpc ($\Lambda\mathrm{CDM}_2$). The study of the nonlinear dark matter density field in $\Lambda\mathrm{CDM}_1$ was carried out by using four statistically independent realizations of the initial conditions. The particular choice of the smoothing scale $R = 1h^{-1}$ Mpc—somewhat smaller than the scale that just has entered the nonlinear regime—allows us to probe the appreciably nonlinear regime. Filtering the nonlinear field on a larger scale, with $R = 10h^{-1}$ Mpc, approximately extracts the underlying linear density field. As mentioned in the Introduction, the large-scale structure of the density field at any given epoch is determined basically by the linear power spectrum on the scales that have just become nonlinear [15–17].

The nonlinear evolution is followed using an N-body particle-mesh code [29], in a simulation cube of side $341.3h^{-1}$ Mpc. The number of particles equals the number of grid points $N_p = N_g = 512^3$, in order to smoothly sample the density field. (The force resolution is adequate given that here we are not interested in the small-scale distribution of matter.) In addition, we also considered two reference power-law models ($n = -2$ and $n = 4$), for each of which 10 realizations were generated. For all four ensembles, the filtering scale was 1.5 times the linear size of a spatial grid cell.

B. Method

Because the initial density field so strongly controls properties of the structure at late times [15–17], we first discuss percolation in Gaussian fields with different $P(k)$, corresponding to four ensemble choices: two with ΛCDM $P(k)$ (parameters as above) and two with power-law spectra $P(k) \propto k^n$ with $n = -2$ and 4. The realizations of the Gaussian density fields were generated by sampling the given amplitude distribution [set by $P(k)$] in k-space, and assuming random phases for individual modes. All the Gaussian fields were generated on a 512^3 spectral grid and then transformed to real space using a fast Fourier transform (FFT). The fields have periodic boundary conditions, and their power spectra necessarily have cutoffs at large (finite mode number) and small wave numbers (finite box size). In terms of normalization, all fields have $\langle\delta\rangle = 0$ and $\sigma_\delta = \langle\delta^2\rangle^{1/2} = 1$. We note, however, that the percolation properties of Gaussian fields depend neither on the mean nor on the variance.

The power spectrum in the ΛCDM model is not a simple power law. Instead, in the limit of small k, $P(k) \propto k$ while in the opposite limit, $P \propto k^{-3}\ln(k/k_c)$, and at the present scale of nonlinearity (roughly), $P \propto k^{-1.5}$ (Fig. 2). In the not so distant past the scale of nonlinearity was smaller and the effective slope was steeper, approximately $n = -2$; in principle this evolutionary stage is observable. The choice

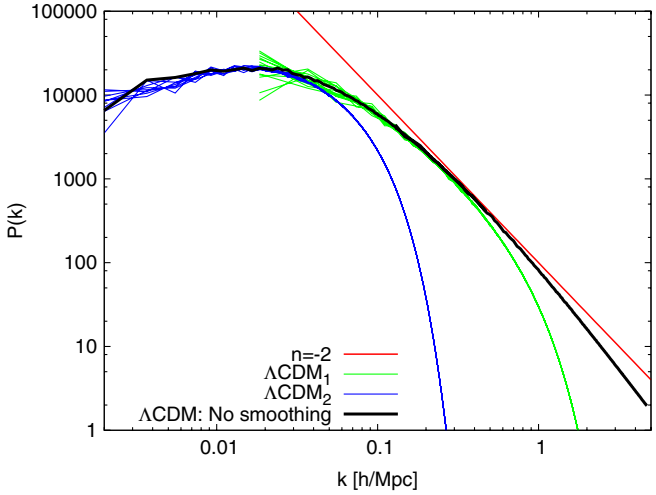

FIG. 2 (color online). Power spectra of two ΛCDM models with smoothing scales, $R = 1$ and $10h^{-1}$ Mpc, and box-sizes 343.1 and $3431h^{-1}$ Mpc, respectively. The unsmoothed ΛCDM power spectrum and $P(k) \propto k^{-2}$ are also shown for reference.

of $n = 4$ corresponds to the so called "minimal power spectrum" on large scales [30] (this power spectrum would arise from initial conditions which have power only on small spatial scales).

Percolating sites are identified using the "friends-of-friends" algorithm on a cubic mesh (only the six closest neighbors were considered as immediate friends) for the (thresholded) density field filtered on a scale R with a Gaussian window. As the density threshold is reduced from a high starting value, the volume in the overdense excursion set increases monotonically until percolation occurs, therefore the volume fraction of the excursion set itself can be used as a proxy for the density threshold. (The same argument also holds for the underdense excursion set.) For the linear density field, percolation curves were averaged over overdense and underdense excursion sets exploiting the exact statistical symmetry of Gaussian fields. The power spectra in the unsmoothed ΛCDM model are shown in Fig. 2 along with the power spectra in all realizations of the $\Lambda\mathrm{CDM}_1$ and $\Lambda\mathrm{CDM}_2$ models; a power-law spectrum with $P(k) \propto k^{-2}$ is also shown for reference.

C. Linear stage

We first focus on the initial stage of structure formation, i.e., any epoch after decoupling of baryonic matter and radiation with only linear density fluctuations on the scales of interest. For the chosen resolution scales (set by the particle number and box size), an initial redshift of $z_i = 50$ comfortably satisfies this criterion.

In order to carry out our percolation analysis we used the volume fraction of the excursion set rather than the density itself as the relevant parameter. We fit the percolation curves by the single-variable percolation scaling ansatz [31]

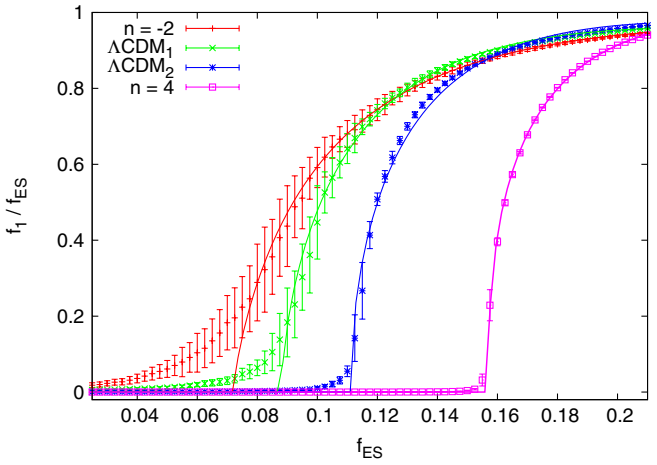

FIG. 3 (color online). Percolation transitions in Gaussian density fields. Results for power-law spectra $P(k) \propto k^n$ with $n = -2$ (extreme left) and $n = 4$ (extreme right), ΛCDM—the two interior curves—smoothed at $R = 1$ (left) and $R = 10h^{-1}$ Mpc (right). Smooth curves are fits to the percolation ansatz (3); error bars are 1σ (statistical).

$$f_1 = A(f_{\rm ES} - f_{\rm p})^{\nu} \quad \text{at } f_{\rm ES} > f_{\rm p}, \tag{3}$$

where $f_{\rm ES}$ is the volume fraction, i.e., the fraction of the volume in the excursion set ($f_{\rm ES} \equiv V_{\rm ES}/V_{\rm tot}$), f_1, the volume fraction of the largest region, and, $f_{\rm p}$, the value of the volume fraction when the percolation transition occurs. In Fig. 3, the quantity, $f_1/f_{\rm ES}$, as numerically determined, is plotted as a function of $f_{\rm ES}$, and undergoes a sudden growth from zero to unity at the percolation transition.

As is evident, the ansatz (3) provides an excellent fit to the data for a power-law model with $n = 4$. Possibly due to finite-volume effects, the fit becomes increasingly less accurate with growth of power on large scales i.e., following the sequence $\Lambda{\rm CDM}_2$, $\Lambda{\rm CDM}_1$, $n = -2$. (We have not been able to identify more rigorous results on percolation in Gaussian fields in the literature.) Establishing precise percolation thresholds will require larger simulation boxes and a more careful analysis of finite-size effects which is beyond the scope of the current paper. However, for our more limited purposes, it is acceptable to use the obtained fitting parameters as fiducial values that characterize the percolation differences in the mutually correlated Gaussian and non-Gaussian fields (the latter having their origin in the nonlinear stage of gravitational instability in the expanding universe). The parameters of the fits are given in Table I.

The data shown in Fig. 3 clearly demonstrate that percolation occurs at lower volume fractions with growth of power on large scales, in qualitative agreement with Ref. [24]. The corresponding density threshold reaches its (lower) limiting value ($\delta_p = \sigma$, $f_{\rm p} = 0.157$), following a conjecture due to Ziman [32] who suggested that the percolation transition should occur exactly at the $\delta = \sigma$ level, for Gaussian fields with dominating small-scale power. At the other extreme considered here, $P(k) \propto k^{-2}$, where the field is dominated by large-scale power, $f_{\rm p} = 0.072$, and corresponds to the highest value of the density threshold $\delta_p/\sigma = 1.46$. This is slightly lower than $\delta_p/\sigma = 1.6 \pm 0.1$ as found in Ref. [24]. The minor disagreement may be due to how the percolation threshold was determined in the two cases, as well as due to finite-volume limitations. [It is also worth noting that our set of fields includes models with nonpower law $P(k)$.] Each parameter in Table I varies monotonically with increase of power on large scales: $f_{\rm p}$ decreases while all the rest increase.

TABLE I. Values for the percolation ansatz (3) parameters (A and ν) for Gaussian fields, the percolation density threshold δ_p corresponds to $f_{\rm p}$, the volume fraction at percolation.

Model	$f_{\rm p}$	A	ν	δ_p/σ
$n = 4$	0.157	0.61	0.38	1.006
$\Lambda{\rm CDM}_2$	0.111	0.66	0.51	1.22
$\Lambda{\rm CDM}_1$	0.089	0.75	0.62	1.36
$n = -2$	0.072	0.89	0.76	1.46

From the results of Fig. 3 it is clear that the percolation transition becomes more gradual as the (effective) spectral index n decreases, deviating from the percolation scaling ansatz at small $f_1/f_{\rm ES}$. Therefore the fit given by Eq. (3) becomes less accurate and $f_{\rm p}$ determined by this method becomes less reliable. This suggests that even larger volumes than the ones used here may be necessary to study such cases. Other factors that may affect the accuracy of the determination of the percolation threshold are discreteness, accuracy of computing the volume of the excursion set, filtering, and the properties of the largest cluster. As the present study is not devoted to an accurate calculation of percolation thresholds in Gaussian fields, we leave these questions to future work.

For scale-free power spectra, $P(k) \propto k^n$, the dependence of the percolation transition in Gaussian fields on the power spectrum was observed and qualitatively discussed in Ref. [23] and then quantified in Ref. [24]. Here, along with two types of scale-free fields, we also study the Gaussian field corresponding to the ΛCDM model smoothed at two different scales (Fig. 2). As mentioned earlier the large-scale structure at the nonlinear stage is mainly determined by the initial power spectrum on scales with $k \lesssim R_{\rm nl}^{-1}$ [15–17] and therefore can be approximately characterized by the effective slope at this scale. It is thus interesting to investigate how well the effective slope at the scales contributing most to the variance of the field determines the percolation transition in the linear regime.

As a first candidate, we study $\Delta^2(k) \equiv k^3 P(k)$, which represents the contribution of power to the variance of the density field, per unit logarithmic interval in k. In particu-

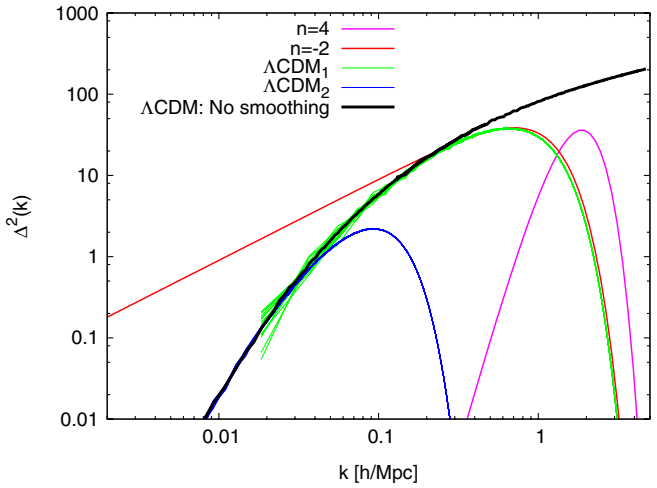

FIG. 4 (color online). The function $\Delta^2(k) = k^3P(k)$ plotted for the power spectra shown in Fig. 2. The power-law spectra with $n = -2$ and $n = 4$ are smoothed with the same window as the $\Lambda\mathrm{CDM}_1$ model. The normalization of $\Delta^2(k)$ is not important since it determines only the variance of the field σ.

lar, the position of the maximum of $\Delta^2(k)$ corresponds to the wavelength with maximum contribution to the variance of the field. Figure 4 shows that the maximum contribution arises from $k \approx 0.65$ and $0.09h$ Mpc^{-1} for the $\Lambda\mathrm{CDM}_1$ and $\Lambda\mathrm{CDM}_2$ models, respectively. The initial i.e., unsmoothed spectrum has the corresponding effective slopes $n_{\mathrm{eff}} = d\log P/d\log k \approx -2.2$ and -1.4 at these wave numbers. The Gaussian field with power-law spectrum $n = 4$ is generated by Fourier waves in a narrow range of k due to the steep falloff in $\Delta^2(k)$ at small wave numbers $\Delta^2(k) \propto k^7$, and Gaussian filtering at small scales.

Referring to Table I, two subsets of the models represented there—one subset consisting of the power-law model with $n = -2$, $\Lambda\mathrm{CDM}_2$ with $n_{\mathrm{eff}} = -1.4$, and the power-law model with $n = 4$, the other consisting of $\Lambda\mathrm{CDM}_1$ with $n_{\mathrm{eff}} = -2.2$, $\Lambda\mathrm{CDM}_2$ with $n_{\mathrm{eff}} = -1.4$, and the power-law model with $n = 4$, both demonstrate monotonic growth of the percolation volume fraction with increase of effective slope: $f_{\mathrm{p}} = 0.07, 0.11, 0.16$ and $f_{\mathrm{p}} = 0.09, 0.11, 016$, respectively. However, percolation in the $\Lambda\mathrm{CDM}_1$ model with $n_{\mathrm{eff}} = -2.2$ formally takes place at a higher value of the volume fraction, $f_{\mathrm{p}} = 0.09$, than for the power-law model with $n = -2$, where $f_{\mathrm{p}} = 0.07$. Regardless of the limited accuracy inherent in measuring the values of f_{p} from the percolation ansatz (3), it does appear reliable to conclude directly from the data points of Fig. 3 that the percolation transition in the power-law model with $n = -2$ occurs at a lower volume fraction than in the $\Lambda\mathrm{CDM}_1$ model. Additionally, the data in Fig. 2 show that the effective slope of the unsmoothed ΛCDM model is slightly more negative than $n = -2$ at $k \approx 0.9h$ Mpc^{-1} (where $\Delta^2(k)$ peaks for the $n = -2$ power spectrum). A more robust measure of the percolation transition threshold is the volume fraction of the excursion set when the volume of the largest cluster comprises half of the excursion set. Table III demonstrates a monotonic decrease of this measure in the order $n = 4$, $\Lambda\mathrm{CDM}_2$, $\Lambda\mathrm{CDM}_1$, and $n = -2$.

An alternative possibility is to use the power per equal interval in k rather than in $\log k$, i.e., $E(k) = k^2P(k)$ instead of $\Delta^2(k) = k^3P(k)$; the former choice being widely used in the theory of turbulence [33]. Again, by finding the maximum of $E(k)$ and then the effective slope in the unsmoothed spectra at these points, one finds that all four models listed in ascending order of f_{p} (i.e., $n = -2$, $\Lambda\mathrm{CDM}_1$, $\Lambda\mathrm{CDM}_1$, and $n = 4$) correspond to monotonically increasing effective slopes, $n_{\mathrm{eff}} = -2, -1.97, -1.1$, and 4. The difference in n_{eff} between the power-law model with $n = -2$ and the $\Lambda\mathrm{CDM}_1$ model is obviously marginal, but the effective slopes at the maxima of $E(k)$ do appear to correspond better to the volume fractions at percolation. The maxima of $E(k)$ are obviously shifted to smaller k with respect to the maxima of $\Delta^2(k)$, therefore $E(k)$ takes into account power on slightly smaller scales than the scales of the maxima of $\Delta^2(k)$. A more detailed evaluation of this issue is a topic for further study and beyond the scope of the current work.

Despite the qualifications in the above discussion, the ΛCDM percolation curves do display trends qualitatively similar to those seen in the bracketing power-law cases. Filtering the density field at smaller scales corresponds to a greater negative effective spectral slope than that due to filtering at larger scales (Fig. 2), the effect of the moving cutoff in k-space leading therefore to a higher density threshold and lower volume fraction at percolation, as demonstrated by the two interior curves in Fig. 3. In particular, this means that the structure formed earlier at greater redshifts was formed from the Gaussian field percolating better than the field corresponding to the current structure.

The dependence of the percolation transition parameters on the power spectrum of a Gaussian field shows that such fields can differ not only locally (e.g., in the shape of peaks, etc. [34]) but also globally. The higher percolation threshold, δ_p, or equivalently lower value of f_{p}, indicates that Gaussian fields with relatively more power on large scales have a greater degree of connectedness. Therefore, the relatively large negative slope of the linear power spectrum at the scale of nonlinearity in the ΛCDM cosmology is an important factor determining the origin of the cosmic web. Because this feature is already present in the initial conditions, later to be amplified by the gravitational instability, we refer to it as the "nature" factor influencing the formation of the cosmic web.

D. Nonlinear stage

Next we turn to a percolation transition analysis of the nonlinear, and therefore non-Gaussian, density field

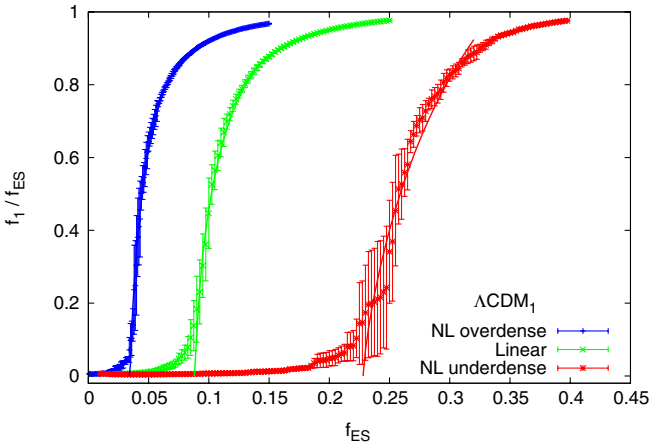

FIG. 5 (color online). $\Lambda\mathrm{CDM}_1$ percolation transitions (filter scale set to $R = 1h^{-1}$ Mpc). Nonlinear stage: overdensity (blue/left) and underdensity (red/right) excursion sets at $z = 0$; linear (Gaussian) stage (green/middle) at $z = 50$. Solid curves are percolation ansatz fits (cf. Eqn. (3) and Table II).

at $z = 0$ for the $\Lambda\mathrm{CDM}_1$ model. As shown in Fig. 5, the percolation threshold for the overdense excursion set at the nonlinear stage (as measured by the volume fraction) is remarkably lower than that for the initial Gaussian field: $f_\mathrm{p}(z = 0) = 0.035$ while $f_\mathrm{p}(z = 50) = 0.089$. This result is as expected from the Zel'dovich approximation [22]. The evolution of the density field results roughly in compression of overdense regions and expansion of underdense regions. This qualitatively correct feature is complicated by the fragmentation of the dense regions into gravitationally bound halos that might make percolation more difficult. However, the relative strength of both effects strongly depends on the power spectrum of the initial Gaussian field. This study suggests that despite the strong fragmentation of the linear percolating region, the overall spatial distribution of the fragments markedly preserves the topology of the linear percolating region, at least in the important case of ΛCDM. The rightmost curve in Fig. 5 shows that the percolation transition in the underdense excursion set occurs at considerably greater volume fraction than in the initial Gaussian field: $f_\mathrm{p}(z = 0) = 0.23$ while $f_\mathrm{p}(z = 50) = 0.089$.

The parameters of the fitting curves are given in Table II. It is worth noting that the percolation transitions in all four tested Gaussian fields are significantly greater than the percolation threshold—measured by volume fraction—for the over-dense phase but smaller than that for the under-dense phase of the nonlinear density field generated by the gravitational instability. Expanding the study of percolation to $n \to -3$ is relatively difficult, therefore whether the above result holds in this limit remains to be seen. It is also worth pointing out that the values of the exponent ν are similar for both overdense and underdense excursion sets, approximately coinciding with the value of ν obtained for the scale-free Gaussian field with $n = -2$. The amplitude A is different in all three cases, however.

TABLE II. Values for the percolation ansatz (Eqn. (3)) parameters for underdense and overdense excursion sets at the nonlinear stage of evolution, the percolation density threshold δ_p corresponds to f_p.

Model	f_p	A	ν	δ_p
NL underdense	0.228	1.80	0.76	−0.80
NL overdense	0.035	0.73	0.75	3.31

TABLE III. Values of f_ES for the fiducial values of $f_1^{(f)}$, (i.e., at the threshold level when $f_1^{(f)} = 0.5 f_\mathrm{ES}$) for the four Gaussian fields and underdense and overdense sets of the evolved nonlinear density fields at $z = 0$.

Model	$f_\mathrm{ES} \pm \sigma_{f_\mathrm{ES}}$
NL underdense	$0.251^{+0.006}_{-0.006}$
$n = 4$	$0.1625^{+0.0002}_{-0.0002}$
$\Lambda\mathrm{CDM}_2$	$0.1198^{+0.0005}_{-0.0006}$
$\Lambda\mathrm{CDM}_1$	$0.102^{+0.002}_{-0.003}$
$n = -2$	$0.094^{+0.003}_{-0.007}$
NL overdense	$0.044^{+0.002}_{-0.0025}$

Compared to the linear case, the density threshold for percolation in the nonlinear regime is significantly larger. (The mean values and standard deviations are obtained from four realizations of the nonlinear stage and 30 realizations of the linear Gaussian field.) A visual comparison can be made by comparing the nonlinear and linear percolating clusters. These are shown in Figs. 6 and 7. Each figure shows a superposition of two stages: linear at $z = 50$ and nonlinear at the present time i.e., at $z = 0$. In each figure, blue and yellow represent initial ($z = 50$) and final ($z = 0$) distributions of mass, respectively. In Fig. 6, the cluster that percolates at $z = 50$ (blue) is transformed into disjoint clumps (yellow) in the course of gravitational evolution as it reaches the present epoch at $z = 0$. The cluster that percolates at $z = 0$ is shown in Fig. 7 in yellow while the distribution of its mass at the linear stage is shown in blue. The masses in the yellow and blue structures are the same in each figure. However, the total mass in the nonlinear percolating cluster—a portion of which is shown in Fig. 7—is about 15 times greater than that in the corresponding linear cluster (shown in Fig. 6): the mass fraction $M_1 \approx 0.25$ at $z = 0$, while $M_1 \approx 0.018$ at $z = 50$.

III. MAPPING ACCURACY

Standard Eulerian perturbation theory at linear order does not move particles. However, if one takes the percolating cluster in the linear density field, smooths it at the scale of nonlinearity, and maps it using the Zel'dovich approximation then in effect one has a (linear theory) prediction for the nonlinear percolating cluster.

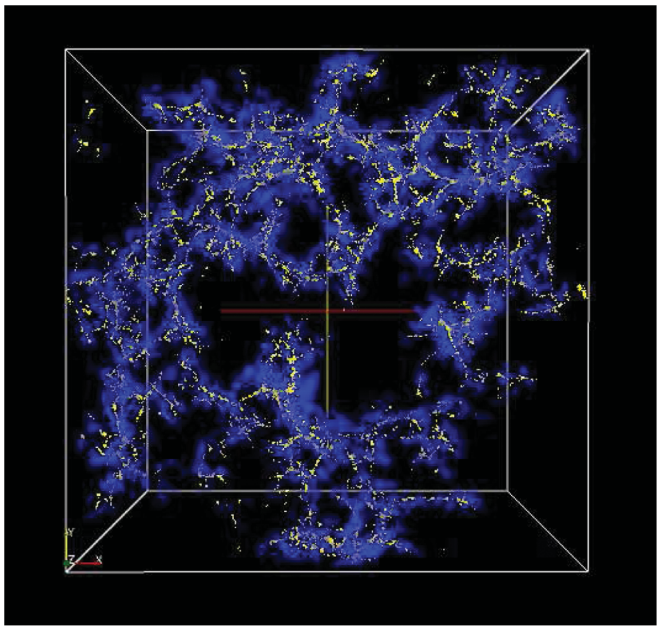

FIG. 6 (color). Forward mapping of the linear percolating cluster. The mapping takes the percolating region identified in the linear regime at $z = 50$ (blue) to the final forward-mapped region at $z = 0$ (yellow, see text). Note the fragmentation of the initial percolating region after the mapping. For visual clarity, a $70h^{-1}$ Mpc thick slab cut out of the full simulation cube is shown.

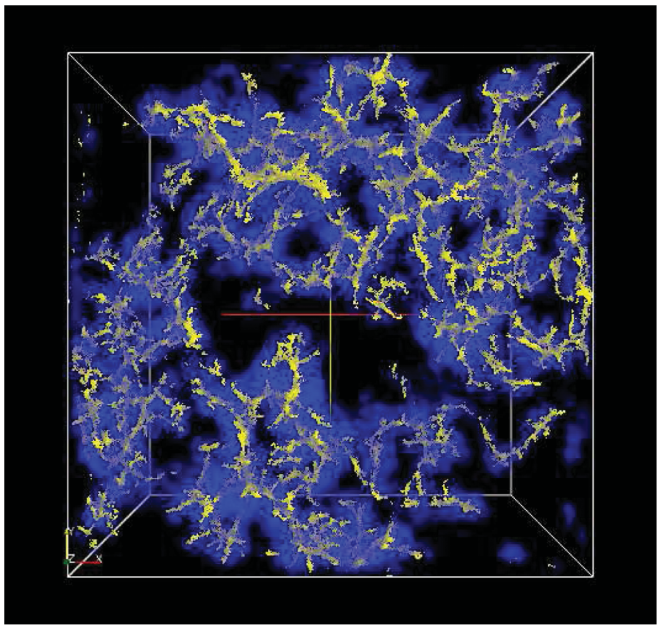

FIG. 7 (color). Backward mapping of the percolating region identified in the nonlinear regime at $z = 0$ (yellow) to the initial stage at $z = 50$ (blue). In contrast to the case of the forward map, the backwards map takes a percolating region into another percolating region. The slab is the same as in Fig. 6.

Intuitively, one may expect that the percolating cluster in the linear field should approximately map into the exact nonlinear percolating cluster, but the accuracy of this proposition has not been directly tested. In this section, we focus on whether the linear percolating cluster indeed maps onto the nonlinear percolating cluster.

We begin by considering the mapping from the initial, linear stage of the evolution ($z = 50$), to the final nonlinear stage ($z = 0$), the *forward map*. This requires two additional steps. First, we choose a fiducial value for the density threshold, $\delta^{(f)}$, to carry out the percolation analysis. We set this to correspond to the point where the largest percolating region occupies 50% of the excursion set volume, i.e., $f_1^{(f)}/f_{\rm ES} = 0.5$. With this choice, the percolation region is well developed, yet not completely dominating the excursion set. This definition is different from that used in the previous analysis (which followed the conventional practice in percolation theory). Therefore the values of $f_{\rm ES}$ for this choice of $f_1^{(f)}$ (see Table III) are a little higher than the values of $f_{\rm p}$ in Tables I and II as expected. The reason for this change is dictated by the fact that at the (conventional) percolation transition, the percolating cluster occupies an infinitesimal volume ($f_1/f_{\rm ES} \to 0$). This means that in a finite box its volume is much smaller than the volume of the box and is thus subject to very large fluctuations. Our choice makes the definition of the percolating cluster more robust and less subject to the precise "turn-on" of percolation (cf. Figs. 3 and 5).

The second step involves multiple back and forth switching from density fields defined on an invariant spatial grid to particles subject to dynamic motion. Although the percolation analysis can be carried out on a set of points it is numerically more efficient on a regular grid. In this study we used a very fast algorithm that detects the percolation transition by performing the cluster analysis on the grid [31]. In particular, it defines the percolating cluster as a set of grid sites. In order to study the forward mapping of the initial percolating cluster (identified as a set of grid sites), we first need to determine the set of particles that are associated with it. Following the motion of these selected particles will allow us to study how the initial percolating region maps into the nonlinear stage.

As a definition, the initial percolating set is taken to be all those particles lying within a distance smaller than half a grid unit (along all three orthogonal axes) from any grid site that belongs to the initial percolating region. After mapping particles to the final nonlinear state we find all the sites on the grid that satisfy the very same criterion. The set of these new sites at $z = 0$ approximates the map of the initial percolating cluster and can be analyzed by the same fast method. We stress that this forward mapping of the linear percolating cluster comprises only a relatively small fraction of particles in the nonlinear percolating cluster because a fundamental feature of the nonlinear evolution is the crossing of orbits and the resulting formation of multi-

stream flow regions. The forward mapping of the percolating cluster found in the linear density field forms only a fraction of those streams, and many others come from regions beyond it. In a similar manner, by starting with the nonlinear percolating cluster at $z = 0$, we introduce a *backward* mapping that finds *all* sites at $z = 50$ that were mapped to $z = 0$ and formed the nonlinear percolating cluster.

With the particle-based definition of percolation applied to the $\Lambda\mathrm{CDM}_1$ cosmology, we find that the particles in the initial percolating set make up 4.6% of the total number of particles in the excursion set—quite close to the volume fraction of the percolating region as defined on the grid (0.045). The small excess is due to the higher than mean density in the percolating region: the two definitions of a percolating region (on grid and by particles) are not identical. But we do expect them to be very similar during the linear stage of the evolution. To verify this expectation we go back from the selected particles to the grid by identifying every grid site closer than half a grid unit to any particle from the percolating set. We then perform a cluster analysis on these sites. Ideally we would find exactly the same grid sites as in the initial percolating cluster. The actual results show good but not perfect correspondence between the two procedures.

Figure 6 illustrates the forward mapping of the initial percolating set (blue) into the nonlinear stage (yellow). Both structures are displayed in comoving coordinates to scale out the uniform Hubble expansion. To avoid excessive projections, every tenth particle is shown in a $70h^{-1}$ Mpc thick slab cut out of the simulation cube. The mapping obviously results in a large reduction of the volume as expected, therefore the nonlinear (yellow) cluster is much smaller by volume than the corresponding linear cluster (blue). A closer look also suggests that the initially connected structure at $z = 50$ becomes fragmented after nonlinear mapping to $z = 0$. We discuss this in more detail below.

In the first step of the analysis, we compute the fraction of particles from the initial percolating set that end up in the final percolating region, as defined on the grid at various thresholds, and shown for the fiducial $\delta^{(f)} = 2.76$ in Fig. 7 in yellow. (We determine whether a particle belongs to the percolating region at $z = 0$ using the same criterion of proximity of particles to grid sites as above, filtering the nonlinear density field also at $R = 1h^{-1}$ Mpc.) The fraction of particles from the initial percolating set transported into the final percolating region is plotted as a function of the ratio $f_1/f_{\mathrm{ES}}(z = 0)$, characterizing the size of the percolating cluster at $z = 0$, in Fig. 8. This fraction grows monotonically from about 40% at $f_1/f_{\mathrm{ES}}(z = 0) \approx 0.22$ to more than 95% at $f_1/f_{\mathrm{ES}}(z = 0) \approx 0.8$ reaching about 80% at the fiducial value $f_1^{(f)}/f_{\mathrm{ES}}(z = 0) = 0.5$. The point of this result is that the progenitor of the "cosmic web" defined as the percolating cluster of the initial

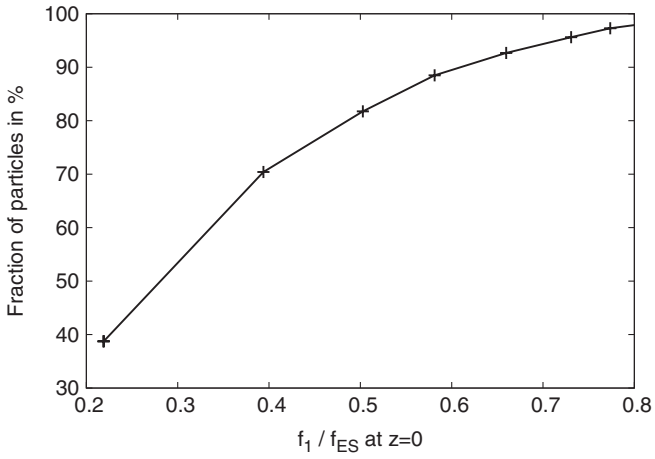

FIG. 8. Fraction of the particles from the initial percolating set ($z = 50$) in the percolating region at $z = 0$ as a function of f_1/f_{ES} at $z = 0$.

Gaussian density field, is a fair, albeit not perfect, "backbone" of the web at a later, nonlinearly evolved stage.

It is also of interest to investigate the percolation properties of the initial set of percolating particles at the final stage of evolution. Using the criterion described above, we generated the set of grid sites at $z = 0$ close to the selected particles (those representing the percolating cluster at $z = 50$) after they had moved to their final positions at $z = 0$. We find that these sites comprise a fraction of less than 0.003 of the total volume. This should be compared with their initial volume occupation fraction of 0.045 at $z = 50$, resulting in a compression factor of about 15 on average. This compression reflects the fact that overdense regions tend to collapse and therefore more than one particle becomes associated by the proximity criterion to the same site at the nonlinear stage. This is clearly seen in Fig. 6. By $z = 0$, the initially connected region fragments into large numbers ($\sim 2.5 \times 10^4$) of isolated regions and none of them percolates. The largest such region has a volume of $\sim 2000h^{-3}$ Mpc^3. Although this volume is quite large by astronomical standards (albeit much smaller than that set by the scale of homogeneity which has a linear dimension of $\sim 70h^{-1}$ Mpc), it comprises only 0.017 of the volume occupied by the particles from the initial percolating set after they are mapped to $z = 0$. These numbers illustrate the prolific fragmentation of the linear percolating cluster in the course of the nonlinear mapping.

We now take the percolating region at $z = 0$, shown in Fig. 7 in yellow, back to the linear stage—the *backward map* (blue region in Fig. 7 with every twentieth particle plotted). As an example, we select the percolating region built from the smoothed density field at $\delta_f = 2.76$ corresponding to $f_1^{(f)}/f_{\mathrm{ES}}(z = 0) = 0.5$. This occupies $8.4 \times 10^5 h^{-3}$ Mpc^3 or 0.02 of all grid sites or equivalently about 0.02 of the volume of the box. The remaining half of the excursion set consists of $\sim 2 \times 10^4$ isolated regions. It is

worth stressing that approximating the percolating region at the nonlinear stage by the particle set as described above, we find that the two representations (particle vs grid) differ considerably more than they do in the linear regime. This is because the particle representation has a significantly higher resolution than the smoothed density field on the grid. In any case, the backward map must be applied using the particle representation; inverse mapping the particles from the largest percolating set back to the linear stage, we find that they occupy about a quarter of the total volume and also form a percolating region (in contrast to the case of the forward map).

IV. SUMMARY

We now summarize our key results. We began by confirming—with some minor discrepancies—earlier findings of the dependence of the percolation threshold in Gaussian random fields on the power spectrum. However, the main purpose of our study is to establish the existence of strong percolation in the initial/linear density field in the ΛCDM cosmological model—the *nature* factor in the formation of the cosmic web. This factor is determined exclusively by the density (or density contrast) field, $\delta \equiv (\rho - \bar{\rho})/\bar{\rho}$ in Eulerian linear theory.

We found that the nonlinear mapping from the linear stage of cosmic evolution ($z = 50$) to the final nonlinear stage at the current epoch ($z = 0$) results in a considerable amplification of percolation features: the percolation volume fraction reduces from $f_{\rm p}(z = 50) \approx 0.09$ to $f_{\rm p}(z = 0) \approx 0.035$, the half-fill volume of the percolating cluster at the fiducial percolation volume fraction reduces from $f_1^{(f)}(z = 50) \approx 0.05$ to $f_1^{(f)}(z = 0) \approx 0.02$, while its mass greatly increases from $m_1^{(f)}(z = 50) \approx 0.025$ to $m_1^{(f)}(z = 0) \approx 0.25$. All these parameter values indicate that the cosmic web becomes considerably thinner and more conspicuous than its progenitor in the linear density field. We call this dynamical influence of the gravitational instability, the *nurture* factor in the formation of the cosmic web because it was not present in the initial field and results entirely from the mapping itself. Conventional linear theory does not consider mapping at all; the Zel'dovich approximation suggests that the initial displacement field, $\mathbf{s} = -\partial\Phi_{\rm lin}/\partial\mathbf{q}$ smoothed at the current scale of nonlinearity determines the dominant features of the mapping.

We conclude that the robust contrast of network structure—so characteristic of N-body simulations—is determined by a combination of two factors: the already-present conspicuousness of the percolating region in the initial Gaussian field (*nature*) and the effects of nonlinear mapping (*nurture*). The first is quantified by the relatively high density threshold ($\delta^{(f)} = 1.27\sigma$) and low volume fraction of the excursion set ($f^{(f)} \approx 0.1$) at the percolation transition. This is directly related to the character of the linear power spectrum—a relatively large negative effective slope in the relevant range of scales from $k = 0.1$ to $1h$ Mpc^{-1}. The second factor is measured by the further decrease of the volume fraction ($f^{(f)} \approx 0.05$) at percolation. The percolation threshold in the density field filtered on $R = 1h^{-1}$ Mpc is $\delta^{(f)} = 2.76$ with the percolating region containing about a quarter of the total mass. We conclude that the nurture factor arising from the dynamical mapping itself is more important for explaining the conspicuousness of the cosmic web.

The topology of the web can also be quantified by the Euler characteristic, but is not equivalent to percolation statistics [35]. In particular, the density of the Euler characteristic, χ, as a function of the level, $\nu = \delta/\sigma_\delta$ has the universal shape, $n_\chi = N_\chi(\nu^2 - 1)\exp(-\nu^2/2)$ for all Gaussian fields regardless of the power spectrum [36]. The power spectrum determines only its amplitude, $N_\chi = 2(\langle k^2\rangle/3)^{3/2}/(2\pi)^2$, where $\langle k\rangle^2 = \int k^2 P(k) k^2 dk / \int P(k) k^2 dk$ [34]. Thus, the standard diagnostics used in cosmology for characterization of the structure: "meatball shift", $\Delta\nu$, "number of voids", A_V, and "number of clusters", A_C (see e.g., Ref. [37]) designed for studies of non-Gaussian features of the structure are unable to detect the "nature" factor in structure formation.

We note that the mapping of the linear percolating cluster into the nonlinear stage is not flawless. The percolating region at the nonlinear stage taken at the half-fill percolation volume fraction contains about 80% of the percolating region found in the linear density field, also taken at the half-fill percolation volume fraction. This is close, though not perfect, correspondence. The half-fill linear percolating cluster makes up about 5%, while the nonlinear one about a quarter, of the total mass, i.e., 5 times greater. The initial percolating region fragments in the course of evolution into a large number (more than 2.5×10^4 in the current simulation) of isolated clumps by $z = 0$, none of which percolates at $z = 0$.

ACKNOWLEDGMENTS

S. S. acknowledges sabbatical support at Los Alamos National Laboratory. S. H. and K. H. acknowledge support from LANL's LDRD and institutional open supercomputing programs. This research was initiated at the Aspen Center for Physics in 2005.

[1] S. A. Gregory and L. A. Thompson, Astrophys. J. **222**, 784 (1978); G. Chincarini and H. Rood, Astrophys. J. **230**, 648 (1979); V. de Lapparent, M. J. Geller, and J. P. Huchra, Astrophys. J. **302**, L1 (1986); H. Lin *et al.*, Astrophys. J. **464**, 60 (1996).

[2] J. K. Adelman-McCarthy *et al.*, Astrophys. J. Suppl. Ser. **172**, 634 (2007).

[3] M. Colless *et al.*, Mon. Not. R. Astron. Soc. **328**, 1039 (2001).

[4] M. U. SubbaRao, M. A. Aragón-Calvo, H. W. Chen, J. M. Quashnock, A. S. Szalay, and D. G. York, New J. Phys. **10**, 125015 (2008).

[5] H. Totsui and T. Kihara, Publ. Astron. Soc. Jpn. **21**, 221 (1969).

[6] P. J. E. Peebles, *The Large Scale Structure of the Universe* (Princeton University Press, Princeton, 1980).

[7] K. Heitmann, M. White, C. Wagner, S. Habib, and D. Higdon, arXiv:0812.1052 [Astrophys. J. (to be published)].

[8] J. R. Gott III, M. Dickinson, and A. L. Melott, Astrophys. J. **306**, 341 (1986).

[9] K. R. Mecke, T. Buchert, and H. Wagner, Astron. Astrophys. **288**, 697 (1994); J. V. Sheth, V. Sahni, S. F. Shandarin, and B. S. Sathyaprakash, Mon. Not. R. Astron. Soc. **343**, 22 (2003).

[10] S. D. M. White, Mon. Not. R. Astron. Soc. **186**, 145 (1979).

[11] J. D. Barrow, S. P. Bhavsar, and D. H. Sonda, Mon. Not. R. Astron. Soc. **216**, 17 (1985).

[12] Ya. B. Zel'dovich, Astron. Astrophys. **5**, 84 (1970).

[13] S. F. Shandarin and Ya. B. Zel'dovich, Rev. Mod. Phys. **61**, 185 (1989).

[14] V. I. Arnold, S. F. Shandarin, and Ya. B. Zel'dovich, Geophys. Astrophys. Fluid Dyn. **20**, 111 (1982).

[15] B. Little, D. H. Weinberg, and C. Park, Mon. Not. R. Astron. Soc. **253**, 295 (1991).

[16] P. Coles, A. L. Melott, and S. F. Shandarin, Mon. Not. R. Astron. Soc. **260**, 765 (1993).

[17] A. L. Melott, T. F. Pellman, and S. F. Shandarin, Mon. Not. R. Astron. Soc. **269**, 626 (1994).

[18] J. R. Bond, L. Kofman, and D. Pogosyan, Nature (London) **380**, 603 (1996).

[19] Ya. B. Zel'dovich, Sov. Astron. Lett. **8**, 102 (1982).

[20] S. F. Shandarin and Ya. B. Zel'dovich, Comments Astrophys. **10**, 33 (1983).

[21] S. F. Shandarin, Sov. Astron. Lett. **9**, 104 (1983).

[22] S. F. Shandarin and Ya. B. Zeldovich, Phys. Rev. Lett. **52**, 1488 (1984).

[23] C. Yess and S. F. Shandarin, Astrophys. J. **465**, 2 (1996).

[24] S. Colombi, D. Pogosyan, and T. Souradeep, Phys. Rev. Lett. **85**, 5515 (2000).

[25] A. Klypin and S. F. Shandarin, Astrophys. J. **413**, 48 (1993).

[26] See, e.g., A. A. Berlind, D. H. Weinberg, A. J. Benson, C. M. Baugh, S. Cole, R. Daveé, C. S. Frenk, A. Jenkins, N. Katz, and C. G. Lacey, Astrophys. J. **593**, 1 (2003).

[27] Ya. B. Zel'dovich, J. Einasto, and S. F. Shandarin, Nature (London) **300**, 407 (1982); J. Einasto, A. A. Klypin, J. Saar, and S. F. Shandarin, Mon. Not. R. Astron. Soc. **206**, 529 (1984); S. F. Shandarin and C. Yess, Astrophys. J. **505**, 12 (1998); S. Bharadwaj, S. P. Bhavsar, and J. V. Sheth, Astrophys. J. **606**, 25 (2004); M. Einasto *et al.*, Astron. Astrophys. **476**, 697 (2007); Astrophys. J. **685**, 83 (2008); T. Sousbie *et al.*, Astrophys. J. **672**, L1 (2008); N. A. Bond, M. A. Strauss, and R. Cen, arXiv:0903.3601; B. J. T. Jones, F. van de Weygaert, and M. A. Aragon-Calvo, arXiv:1001.4479; E. Choi *et al.*, arXiv:1003.3239.

[28] N. Kaiser, Mon. Not. R. Astron. Soc. **227**, 1 (1987); S. Shandarin, J. Cosmol. Astropart. Phys. 02 (2009) 031.

[29] K. Heitmann, P. M. Ricker, M. Warren, and S. Habib, Astrophys. J. Suppl. Ser. **160**, 28 (2005).

[30] A. G. Doroshkevich and Ya. B. Zel'dovich, Astrophys. Space Sci. **35**, 55 (1975).

[31] D. Stauffer and A. Aharony, *Introduction to Percolation Theory* (Taylor and Francis, London, 1992), Ch. III and associated references.

[32] J. M. Ziman, *Models of Disorder* (Cambridge University Press, Cambridge, England, 1979).

[33] A. S. Monin and A. M. Yaglom, *Statistical Fluid Mechanics: Mechanics of Turbulence* (The MIT Press, Cambridge, MA, 1975), Vol. 2.

[34] J. M. Bardeen, J. R. Bond, N. Kaiser, and A. S. Szalay, Astrophys. J. **304**, 15 (1986).

[35] V. Sahni, B. S. Sathyaprakash, and S. F. Shandarin, Astrophys. J. **476**, L1 (1997).

[36] A. G. Doroshkevich, Astrophys. J. **6**, 320 (1970).

[37] J. R. Gott III, Y. Y. Choi, C. Park, and J. Kim, Astrophys. J. **695**, L45 (2009).